Chapter 20 / Materials Selection and Design Considerations

Shown in this photograph is the landing of the *Atlantis* Space Shuttle Orbiter. This chapter discusses the materials that are used for its outer airframe's thermal protection system. [Photograph courtesy the National Aeronautics and Space Administration (NASA).]

Why Study *Materials Selection and Design Considerations?*

Perhaps one of the most important tasks that an engineer may be called upon to perform is that of materials selection with regard to component design. Inappropriate or improper decisions can be disastrous from both economic and safety perspectives. Therefore, it is essential that the engineering student become familiar with and versed in the procedures and protocols that are normally employed in this process. This chapter discusses materials selection issues in several contexts and from various perspectives.

Learning Objectives

After careful study of this chapter you should be able to do the following:

1. **Describe how the strength performance index for a solid cylindrical shaft is determined.**
2. **Describe the manner in which materials selection charts are employed in the materials selection process.**
3. **Briefly describe the steps that are used to ascertain whether or not a particular metal alloy is suitable for use in an automobile valve spring.**
4. **List and briefly explain six biocompatibility considerations relative to materials that are employed in artificial hip replacements.**
5. **Name the four components found in the artificial hip replacement, and, for each, list its specific material requirements.**
6. **(a) Name the three components of the thermal protection system for the Space Shuttle Orbiter. (b) Describe the composition, microstructure, and general properties of the ceramic tiles that are used on the Space Shuttle Orbiter.**
7. **Describe the components and their functions for an integrated circuit leadframe.**
8. **(a) Name and briefly describe the three processes that are carried out during integrated circuit packaging. (b) Note property requirements for each of these processes, and, in addition, cite at least two materials that are employed.**

20.1 Introduction

Virtually the entire book to this point has dealt with the properties of various materials, how the properties of a specific material are dependent on its structure, and, in many cases, how structure may be fashioned by the processing technique that is employed during production. Of late, there has been a trend to emphasize the element of *design* in engineering pedagogy. To a materials scientist or materials engineer, design can be taken in several contexts. First of all, it can mean designing new materials having unique property combinations. Alternatively, design can involve selecting a new material having a better combination of characteristics for a specific application; choice of material cannot be made without consideration of necessary manufacturing processes (e.g., forming, welding, etc.), which also rely on material properties. Or, finally, design might mean developing a process for producing a material having better properties.

One particularly effective technique for teaching design principles is the case study method. With this technique, the solutions to real-life engineering problems are carefully analyzed in detail so that the student may observe the procedures and rationale that are involved in the decision-making process. We have chosen to perform five case studies which draw upon principles that were introduced in previous chapters. These five studies involve materials that are used for the following: (1) a torsionally stressed cylindrical shaft; (2) an automobile valve spring; (3) the artificial total hip replacement; (4) the thermal protection system on the Space Shuttle Orbiter; and (5) integrated circuit packages.

MATERIALS SELECTION FOR A TORSIONALLY STRESSED CYLINDRICAL SHAFT

We begin by addressing the design process from the perspective of materials selection; that is, for some application, selecting a material having a desirable or optimum property or combination of properties. Elements of this materials selection process involve deciding on the constraints of the problem, and, from these, establishing criteria that can be used in materials selection to maximize performance.

The component or structural element we have chosen to discuss is a solid cylindrical shaft that is subjected to a torsional stress. Strength of the shaft will be

considered in detail, and criteria will be developed for the maximization of strength with respect to both minimum material mass and minimum cost. Other parameters and properties that may be important in this selection process are also discussed briefly.

20.2 Strength

For this portion of the problem, we will establish a criterion for selection of light and strong materials for this shaft. It will be assumed that the twisting moment and length of the shaft are specified, whereas the radius (or cross-sectional area) may be varied. We develop an expression for the mass of material required in terms of twisting moment, shaft length, and density and strength of the material. Using this expression, it will be possible to evaluate the performance—that is, maximize the strength of this torsionally stressed shaft with respect to mass and, in addition, relative to material cost.

Consider the cylindrical shaft of length L and radius r, as shown in Figure 20.1. The application of twisting moment (or torque), M_t produces an angle of twist ϕ. Shear stress τ at radius r is defined by the equation

$$\tau = \frac{M_t r}{J} \tag{20.1}$$

Here, J is the polar moment of inertia, which for a solid cylinder is

$$J = \frac{\pi r^4}{2} \tag{20.2}$$

Thus,

$$\tau = \frac{2M_t}{\pi r^3} \tag{20.3}$$

A safe design calls for the shaft to be able to sustain some twisting moment without fracture. In order to establish a materials selection criterion for a light and strong material, we replace the shear stress in Equation 20.3 with the shear strength of the material τ_f divided by a factor of safety N, as

$$\frac{\tau_f}{N} = \frac{2M_t}{\pi r^3} \tag{20.4}$$

It is now necessary to take into consideration material mass. The mass m of any given quantity of material is just the product of its density (ρ) and volume. Since the volume of a cylinder is just $\pi r^2 L$, then

$$m = \pi r^2 L \rho \tag{20.5}$$

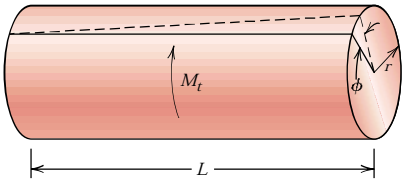

Figure 20.1 A solid cylindrical shaft that experiences an angle of twist ϕ in response to the application of a twisting moment M_t.

Or, the radius of the shaft in terms of its mass is just

$$r = \sqrt{\frac{m}{\pi L \rho}} \tag{20.6}$$

Substitution of this r expression into Equation 20.4 leads to

$$\frac{\tau_f}{N} = \frac{2M_t}{\pi\left(\sqrt{\frac{m}{\pi L \rho}}\right)^3}$$

$$= 2M_t\sqrt{\frac{\pi L^3 \rho^3}{m^3}} \tag{20.7}$$

Solving this expression for the mass m yields

$$m = (2NM_t)^{2/3}(\pi^{1/3}L)\left(\frac{\rho}{\tau_f^{2/3}}\right) \tag{20.8}$$

The parameters on the right-hand side of this equation are grouped into three sets of parentheses. Those contained within the first set (i.e., N and M_t) relate to the safe functioning of the shaft. Within the second parentheses is L, a geometric parameter. And, finally, the material properties of density and strength are contained within the last set.

The upshot of Equation 20.8 is that the best materials to be used for a light shaft which can safely sustain a specified twisting moment are those having low $\rho/\tau_f^{2/3}$ ratios. In terms of material suitability, it is sometimes preferable to work with what is termed a *performance index, P*, which is just the reciprocal of this ratio; that is

$$P = \frac{\tau_f^{2/3}}{\rho} \tag{20.9}$$

In this context we want to utilize a material having a large performance index.

At this point it becomes necessary to examine the performance indices of a variety of potential materials. This procedure is expedited by the utilization of what are termed *materials selection charts.*[1] These are plots of the values of one material property versus those of another property. Both axes are scaled logarithmically and usually span about five orders of magnitude, so as to include the properties of virtually all materials. For example, for our problem, the chart of interest is logarithm of strength versus logarithm of density, which is shown in Figure 20.2.[2] It may be noted on this plot that materials of a particular type (e.g., woods, engineering polymers, etc.) cluster together and are enclosed within an envelope delineated with a bold line. Subclasses within these clusters are enclosed using finer lines.

[1] A comprehensive collection of these charts may be found in M. F. Ashby, *Materials Selection in Mechanical Design,* Pergamon Press, Oxford, 1992.

[2] Strength for metals and polymers is taken as yield strength, for ceramics and glasses, compressive strength, for elastomers, tear strength, and for composites, tensile failure strength.

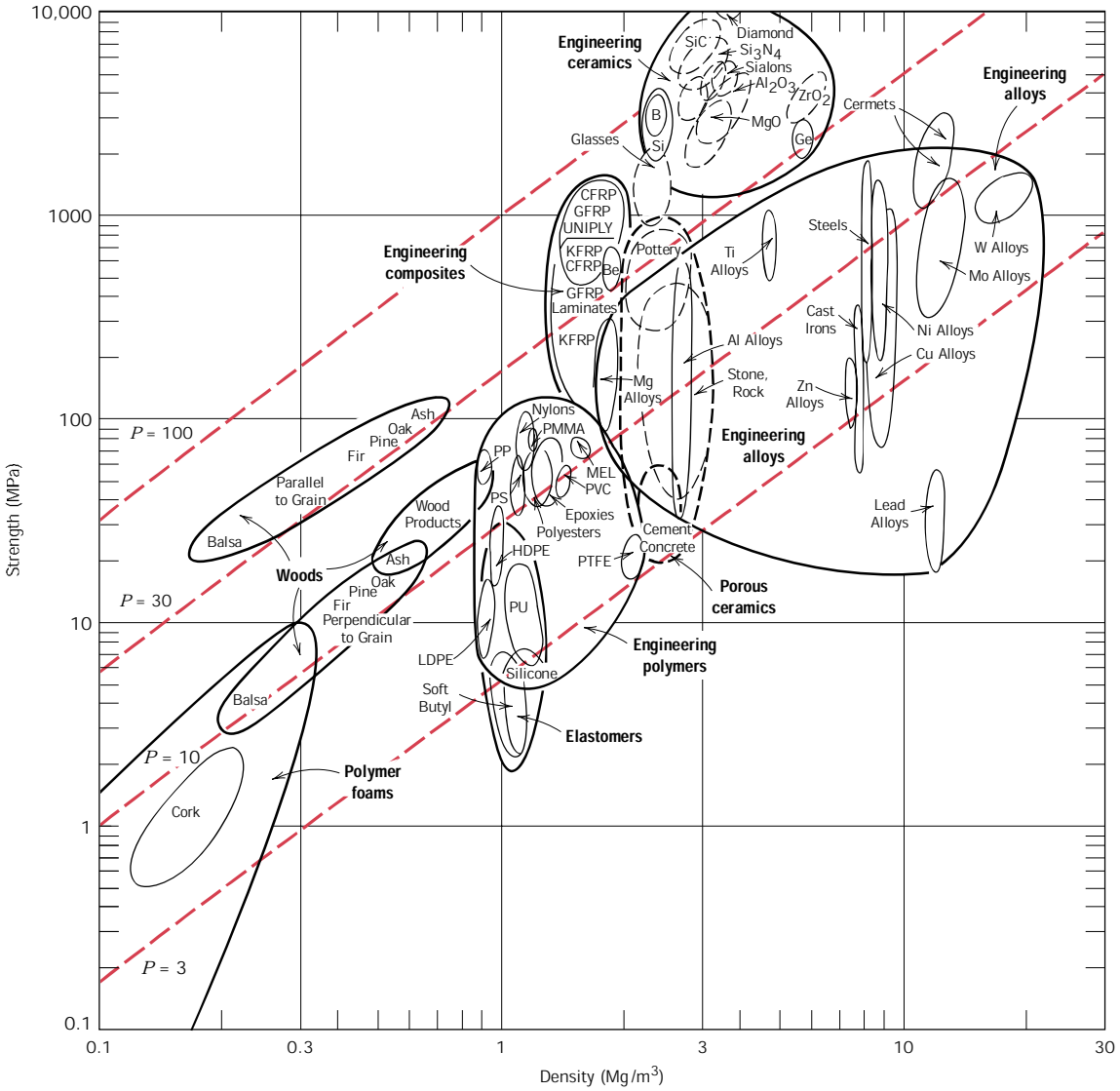

FIGURE 20.2 Strength versus density materials selection chart. Design guidelines for performance indices of 3, 10, 30, and 100 $(MPa)^{2/3}m^3/Mg$ have been constructed, all having a slope of $\frac{3}{2}$. (Adapted from M. F. Ashby, *Materials Selection in Mechanical Design.* Copyright © 1992. Reprinted by permission of Butterworth-Heinemann Ltd.)

Now, taking the logarithm of both sides of Equation 20.9 and rearranging yields

$$\log \tau_f = \tfrac{3}{2} \log \rho + \tfrac{3}{2} \log P \tag{20.10}$$

This expression tells us that a plot of log τ_f versus log ρ will yield a family of straight and parallel lines all having a slope of $\frac{3}{2}$; each line in the family corresponds to a different performance index, P. These lines are termed *design guidelines,* and four

have been included in Figure 20.2 for P values of 3, 10, 30, and 100 $(MPa)^{2/3}m^3/Mg$. All materials that lie on one of these lines will perform equally well in terms of strength-per-mass basis; materials whose positions lie above a particular line will have higher performance indices, while those lying below will exhibit poorer performances. For example, a material on the $P = 30$ line will yield the same strength with one-third the mass as another material that lies along the $P = 10$ line.

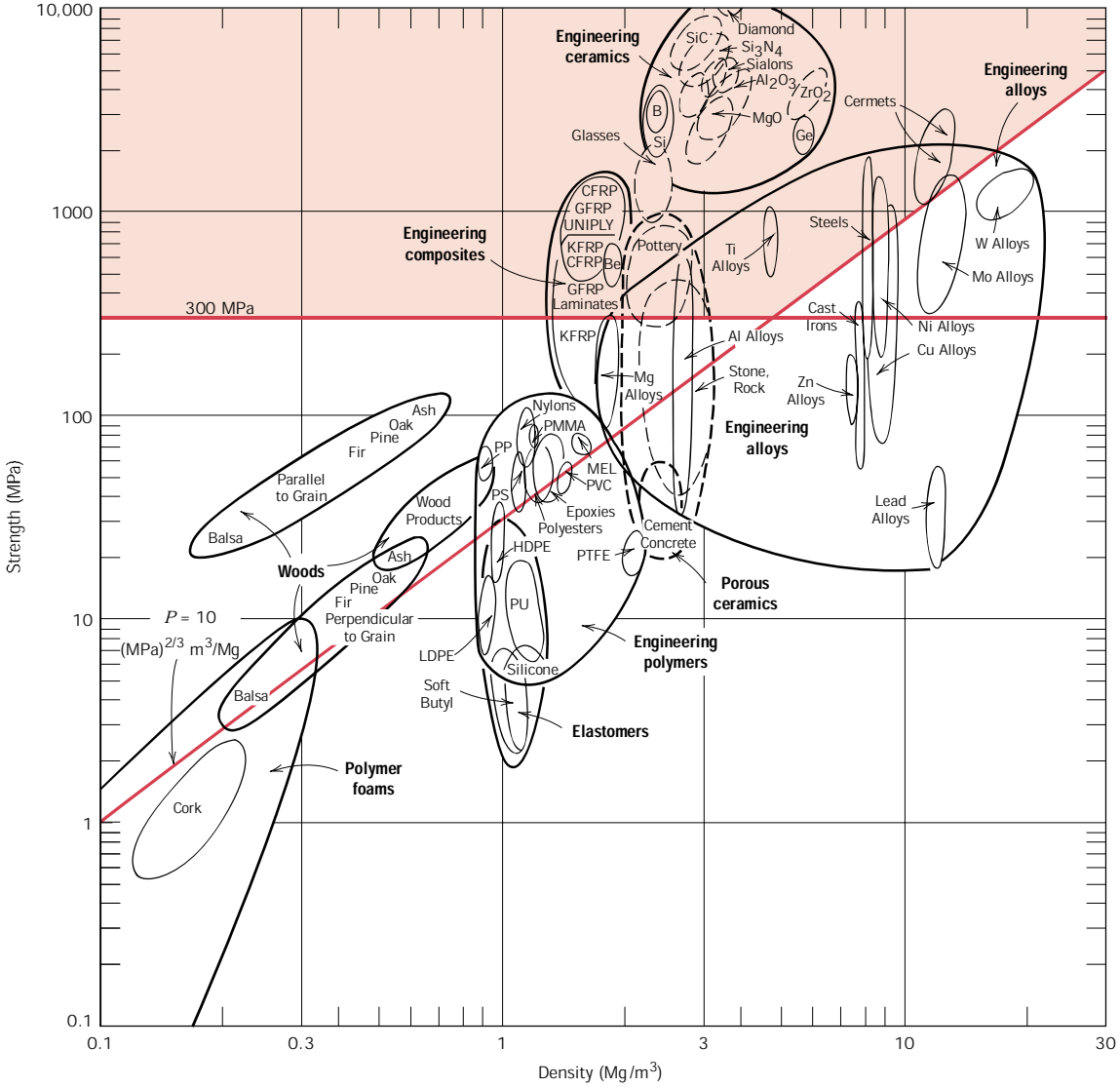

FIGURE 20.3 Strength versus density materials selection chart. Those materials lying within the shaded region are acceptable candidates for a solid cylindrical shaft which has a mass-strength performance index in excess of 10 $(MPa)^{2/3}m^3/Mg$, and a strength of at least 300 MPa (43,500 psi). (Adapted from M. F. Ashby, *Materials Selection in Mechanical Design.* Copyright © 1992. Reprinted by permission of Butterworth-Heinemann Ltd.)

The selection process now involves choosing one of these lines, a ''selection line'' that includes some subset of these materials; for the sake of argument let us pick $P = 10$ (MPa)$^{2/3}$m^3/Mg, which is represented in Figure 20.3. Materials lying along this line or above it are in the ''search region'' of the diagram and are possible candidates for this rotating shaft. These include wood products, some plastics, a number of engineering alloys, the engineering composites, and glasses and engineering ceramics. On the basis of fracture toughness considerations, the engineering ceramics and glasses are ruled out as possibilities.

Let us now impose a further constraint on the problem, namely that the strength of the shaft must equal or exceed 300 MPa (43,500 psi). This may be represented on the materials selection chart by a horizontal line constructed at 300 MPa, Figure 20.3. Now the search region is further restricted to that area above both of these lines. Thus, all wood products, all engineering polymers, other engineering alloys (viz. Mg and some Al alloys), as well as some engineering composites are eliminated as candidates; steels, titanium alloys, high-strength aluminum alloys, and the engineering composites remain as possibilities.

At this point we are in a position to evaluate and compare the strength performance behavior of specific materials. Table 20.1 presents the density, strength, and strength performance index for three engineering alloys and two engineering composites, which were deemed acceptable candidates from the analysis using the materials selection chart. In this table, strength was taken as 0.6 times the tensile yield strength (for the alloys) and 0.6 times the tensile strength (for the composites); these approximations were necessary since we are concerned with strength in torsion and torsional strengths are not readily available. Furthermore, for the two engineering composites, it is assumed that the continuous and aligned glass and carbon fibers are wound in a helical fashion (Figure 15.14), and at a 45° angle referenced to the shaft axis. The five materials in Table 20.1 are ranked according to strength performance index, from highest to lowest: carbon fiber-reinforced and glass fiber-reinforced composites, followed by aluminum, titanium, and 4340 steel alloys.

Material cost is another important consideration in the selection process. In real-life engineering situations, economics of the application often is the overriding issue and normally will dictate the material of choice. One way to determine materi-

Table 20.1 Density (ρ), Strength (τ_f), the Performance Index (P) for Five Engineering Materials

Material	ρ (Mg/m^3)	τ_f (MPa)	$\tau_f^{2/3}/\rho = P$ [$(MPa)^{2/3}m^3/Mg$]
Carbon fiber-reinforced composite (0.65 fiber fraction) [a]	1.5	1140	72.8
Glass fiber-reinforced composite (0.65 fiber fraction) [a]	2.0	1060	52.0
Aluminum alloy (2024-T6)	2.8	300	16.0
Titanium alloy (Ti-6Al-4V)	4.4	525	14.8
4340 Steel (oil-quenched and tempered)	7.8	780	10.9

[a] The fibers in these composites are continuous, aligned, and wound in a helical fashion at a 45° angle relative to the shaft axis.

Table 20.2 Tabulation of the $\rho/\tau_f^{2/3}$ Ratio, Relative Cost ($\overline{c}$), and the Product of $\rho/\tau_f^{2/3}$ and $\overline{c}$ for Five Engineering Materials[a]

Material	$\rho/\tau_f^{2/3}$ $[10^{-2}\ \{Mg/(MPa)^{2/3}m^3\}]$	$\overline{c}$ ($/$)	$\overline{c}(\rho/\tau_f^{2/3})$ $[10^{-2}\ (\$/\$)\{Mg/(MPa)^{2/3}m^3\}]$
4340 Steel (oil-quenched and tempered)	9.2	5	46
Glass fiber-reinforced composite (0.65 fiber fraction)[b]	1.9	40	76
Aluminum alloy (2024-T6)	6.2	15	93
Carbon fiber-reinforced composite (0.65 fiber fraction)[b]	1.4	80	112
Titanium alloy (Ti-6Al-4V)	6.8	110	748

[a] The relative cost is the ratio of the prices per unit mass of the material and low-carbon steel.

[b] The fibers in these composites are continuous, aligned, and wound in a helical fashion at a 45° angle relative to the shaft axis.

als cost is by taking the product of the price (on a per-unit mass basis) and the required mass of material.

Cost considerations for these five remaining candidate materials—steel, aluminum, and titanium alloys, and two engineering composites—are presented in Table 20.2. In the first column is tabulated $\rho/\tau_f^{2/3}$. The next column lists the approximate relative cost, denoted as $\overline{c}$; this parameter is simply the per-unit mass cost of material divided by the per-unit mass cost for low-carbon steel, one of the common engineering materials. The underlying rationale for using $\overline{c}$ is that while the price of a specific material will vary over time, the price ratio between that material and another will, most likely, change more slowly.

Finally, the right-hand column of Table 20.2 shows the product of $\rho/\tau_f^{2/3}$ and $\overline{c}$. This product provides a comparison of these several materials on the basis of the cost of materials for a cylindrical shaft that would not fracture in response to the twisting moment M_t. We use this product inasmuch as $\rho/\tau_f^{2/3}$ is proportional to the mass of material required (Equation 20.8) and $\overline{c}$ is the relative cost on a per-unit mass basis. Now the most economical is the 4340 steel, followed by the glass fiber-reinforced composite, 2024-T6 aluminum, the carbon fiber-reinforced composite, and the titanium alloy. Thus, when the issue of economics is considered, there is a significant alteration within the ranking scheme. For example, inasmuch as the carbon fiber-reinforced composite is relatively expensive, it is significantly less desirable; or, in other words, the higher cost of this material may not outweigh the enhanced strength it provides.

20.3 Other Property Considerations and the Final Decision

To this point in our materials selection process we have considered only the strength of materials. Other properties relative to the performance of the cylindrical shaft may be important—for example, stiffness, and, if the shaft rotates, fatigue behavior. Furthermore, fabrication costs should also be considered; in our analysis they have been neglected.

Relative to stiffness, a stiffness-to-mass performance analysis similar to that above could be conducted. For this case, the stiffness performance index P_s is

$$P_s = \frac{\sqrt{G}}{\rho} \tag{20.11}$$

where G is the shear modulus. The appropriate materials selection chart (log G versus log ρ) would be used in the preliminary selection process. Subsequently, performance index and per-unit-mass cost data would be collected on specific candidate materials; from these analyses the materials would be ranked on the basis of stiffness performance and cost.

In deciding on the best material, it may be worthwhile to make a table employing the results of the various criteria that were used. The tabulation would include, for all candidate materials, performance index, cost, etc. for each criterion, as well as comments relative to any other important considerations. This table puts in perspective the important issues and facilitates the final decision process.

AUTOMOBILE VALVE SPRING

20.4 Introduction

The basic function of a spring is to store mechanical energy as it is initially elastically deformed and then recoup this energy at a later time as the spring recoils. In this section helical springs that are used in mattresses and in retractable pens and as suspension springs in automobiles are discussed. A stress analysis will be conducted on this type of spring, and the results will then be applied to a valve spring that is utilized in automobile engines.

Consider the helical spring shown in Figure 20.4, which has been constructed of wire having a circular cross section of diameter d; the coil center-to-center diameter is denoted as D. The application of a compressive force F causes a twisting force, or moment, denoted T, as shown in the figure. A combination of shear stresses result, the sum of which, τ, is

$$\tau = \frac{8FD}{\pi d^3} K_w \tag{20.12}$$

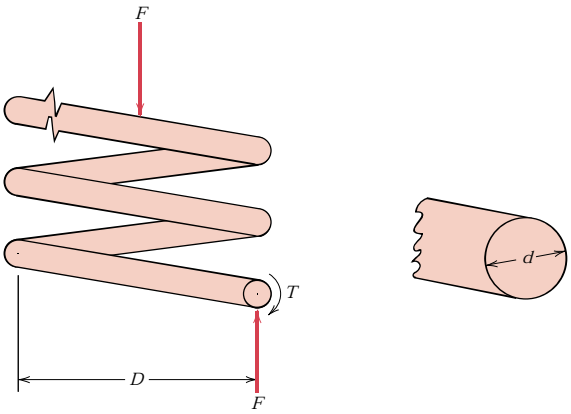

Figure 20.4 Schematic diagram of a helical spring showing the twisting moment T that results from the compressive force F. (Adapted from K. Edwards and P. McKee, *Fundamentals of Mechanical Component Design.* Copyright © 1991 by McGraw-Hill, Inc. Reproduced with permission of The McGraw-Hill Companies.)

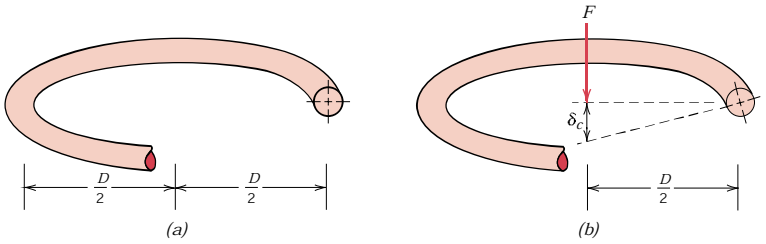

FIGURE 20.5 Schematic diagrams of one coil of a helical spring, (*a*) prior to being compressed, and (*b*) showing the deflection δ_c produced from the compressive force *F*. (Adapted from K. Edwards and P. McKee, *Fundamentals of Mechanical Component Design.* Copyright © 1991 by McGraw-Hill, Inc. Reproduced with permission of The McGraw-Hill Companies.)

where K_w is a force-independent constant that is a function of the D/d ratio:

$$K_w = 1.60\left(\frac{D}{d}\right)^{-0.140} \tag{20.13}$$

In response to the force *F*, the coiled spring will experience deflection, which will be assumed to be totally elastic. The amount of deflection per coil of spring, δ_c, as indicated in Figure 20.5, is given by the expression

$$\delta_c = \frac{8FD^3}{d^4G} \tag{20.14}$$

where *G* is the shear modulus of the material from which the spring is constructed. Furthermore, δ_c may be computed from the total spring deflection, δ_s, and the number of effective spring coils, N_c, as

$$\delta_c = \frac{\delta_s}{N_c} \tag{20.15}$$

Now, solving for *F* in Equation 20.14 gives

$$F = \frac{d^4\delta_c G}{8D^3} \tag{20.16}$$

and substituting for *F* in Equation 20.12 leads to

$$\tau = \frac{\delta_c G d}{\pi D^2}K_w \tag{20.17}$$

Under normal circumstances, it is desired that a spring experience no permanent deformation upon loading; this means that the right-hand side of Equation 20.17 must be less than the shear yield strength τ_y of the spring material, or that

$$\tau_y > \frac{\delta_c G d}{\pi D^2}K_w \tag{20.18}$$

20.5 Automobile Valve Spring

We shall now apply the results of the preceding section to an automobile valve spring. A cut-away schematic diagram of an automobile engine showing these springs is presented in Figure 20.6. Functionally, springs of this type permit both intake and exhaust valves to alternately open and close as the engine is in operation. Rotation of the camshaft causes a valve to open and its spring to be compressed, so that the load on the spring is increased. The stored energy in the spring then forces the valve to close as the camshaft continues its rotation. This process occurs for each valve for each engine cycle, and over the lifetime of the engine it occurs many millions of times. Furthermore, during normal engine operation, the temperature of the springs is approximately 80°C (175°F).

A photograph of a typical valve spring is shown in Figure 20.7. The spring has a total length of 1.67 in. (42 mm), is constructed of wire having a diameter d of 0.170 in. (4.3 mm), has six coils (only four of which are active), and has a center-to-center diameter D of 1.062 in. (27 mm). Furthermore, when installed and when a valve is completely closed, its spring is compressed a total of 0.24 in. (6.1 mm), which, from Equation 20.15, gives an installed deflection per coil δ_{ic} of

$$\delta_{ic} = \frac{0.24 \text{ in.}}{4 \text{ coils}} = 0.060 \text{ in./coil } (1.5 \text{ mm/coil})$$

The cam lift is 0.30 in. (7.6 mm), which means that when the cam completely opens a valve, the spring experiences a maximum total deflection equal to the sum of the valve lift and the compressed deflection, namely, 0.30 in. + 0.24 in. = 0.54 in. (13.7

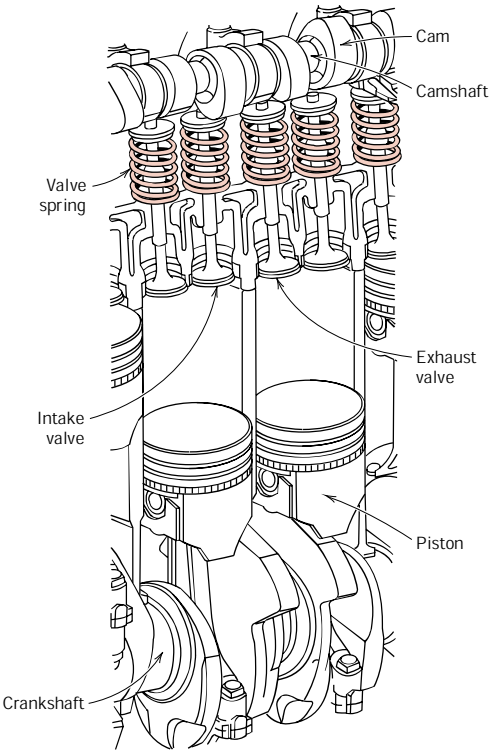

Figure 20.6 Cutaway drawing of a section of an automobile engine in which various components including valves and valve springs are shown.

FIGURE 20.7 Photograph of a typical automobile valve spring.

mm). Hence, the maximum deflection per coil, δ_{mc}, is

$$\delta_{mc} = \frac{0.54 \text{ in.}}{4 \text{ coils}} = 0.135 \text{ in./coil } (3.4 \text{ mm/coil})$$

Thus, we have available all of the parameters in Equation 20.18 (taking $\delta_c = \delta_{mc}$), except for τ_y, the required shear yield strength of the spring material.

However, the material parameter of interest is really not τ_y inasmuch as the spring is continually stress cycled as the valve opens and closes during engine operation; this necessitates designing against the possibility of failure by fatigue rather than against the possibility of yielding. This fatigue complication is handled by choosing a metal alloy that has a fatigue limit (Figure 9.25*a*) that is greater than the cyclic stress amplitude to which the spring will be subjected. For this reason, steel alloys, which have fatigue limits, are normally employed for valve springs.

When using steel alloys in spring design, two assumptions may be made if the stress cycle is reversed (if $\tau_m = 0$, where τ_m is the mean stress, or, equivalently, if $\tau_{max} = -\tau_{min}$, in accordance with Equation 9.21 and as noted in Figure 20.8). The first of these assumptions is that the fatigue limit of the alloy (expressed as stress amplitude) is 45,000 psi (310 MPa), the threshold of which occurs at about 10^6 cycles. Secondly, for torsion and on the basis of experimental data, it has been

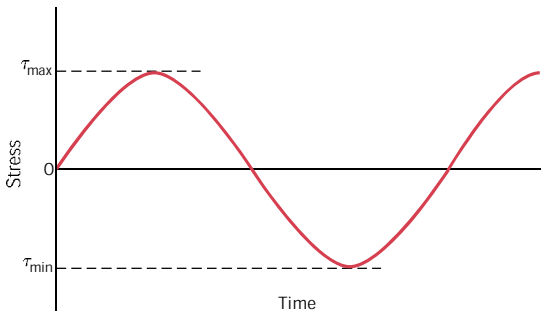

FIGURE 20.8 Stress versus time for a reversed cycle in shear.

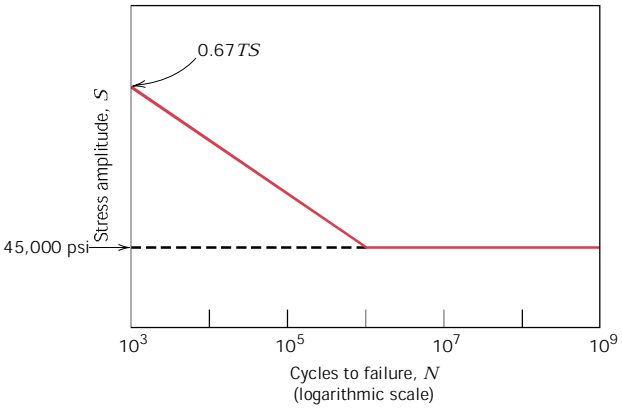

FIGURE 20.9 Shear stress amplitude versus logarithm of the number of cycles to fatigue failure for typical ferrous alloys.

found that the fatigue strength at 10^3 cycles is $0.67TS$, where TS is the tensile strength of the material (as measured from a pure tension test). The S–N fatigue diagram (i.e., stress amplitude versus logarithm of the number of cycles to failure) for these alloys is shown in Figure 20.9.

Now let us estimate the number of cycles to which a typical valve spring may be subjected in order to determine whether it is permissible to operate within the fatigue limit regime of Figure 20.9 (i.e., if the number of cycles exceeds 10^6). For the sake of argument, assume that the automobile in which the spring is mounted travels a minimum of 100,000 miles (161,000 km) at an average speed of 40 mph (64.4 km/h), with an average engine speed of 3000 rpm (rev/min). The total time it takes the automobile to travel this distance is 2500 h (100,000 mi/40 mph), or 150,000 min. At 3000 rpm, the total number of revolutions is (3000 rev/min) (150,000 min) $= 4.5 \times 10^8$ rev, and since there are 2 rev/cycle, the total number of cycles is 2.25×10^8. This result means that we may use the fatigue limit as the design stress inasmuch as the limit cycle threshold has been exceeded for the 100,000-mile distance of travel (i.e., since 2.25×10^8 cycles $> 10^6$ cycles).

Furthermore, this problem is complicated by the fact that the stress cycle is not completely reversed (i.e., $\tau_m \neq 0$) inasmuch as between minimum and maximum deflections the spring remains in compression; thus, the 45,000 psi (310 MPa) fatigue limit is not valid. What we would now like to do is first to make an appropriate extrapolation of the fatigue limit for this $\tau_m \neq 0$ case and then compute and compare with this limit the actual stress amplitude for the spring; if the stress amplitude is significantly below the extrapolated limit, then the spring design is satisfactory.

A reasonable extrapolation of the fatigue limit for this $\tau_m \neq 0$ situation may be made using the following expression (termed Goodman's law):

$$\tau_{al} = \tau_e \left(1 - \frac{\tau_m}{0.67\,TS}\right) \tag{20.19}$$

where τ_{al} is the fatigue limit for the mean stress τ_m; τ_e is the fatigue limit for $\tau_m = 0$ [i.e., 45,000 psi (310 MPa)]; and, again, TS is the tensile strength of the alloy. To determine the new fatigue limit τ_{al} from the above expression necessitates the computation of both the tensile strength of the alloy and the mean stress for the spring.

One common spring alloy is an ASTM 232 chrome–vanadium steel, having a composition of 0.48–0.53 wt% C, 0.80–1.10 wt% Cr, a minimum of 0.15 wt% V, and the balance being Fe. Spring wire is normally cold drawn (Section 14.2) to the desired diameter; consequently, tensile strength will increase with the amount of drawing (i.e., with decreasing diameter). For this alloy it has been experimentally verified that, for the diameter d in inches, the tensile strength is

$$TS\,(\text{psi}) = 169{,}000\,(d)^{-0.167} \tag{20.20}$$

Since $d = 0.170$ in. for this spring,

$$\begin{aligned} TS &= (169{,}000)\,(0.170\ \text{in.})^{-0.167} \\ &= 227{,}200\ \text{psi}\ (1570\ \text{MPa}) \end{aligned}$$

Computation of the mean stress τ_m is made using Equation 9.21 modified to the shear stress situation as follows:

$$\tau_m = \frac{\tau_{\text{min}} + \tau_{\text{max}}}{2} \tag{20.21}$$

It now becomes necessary to determine the minimum and maximum shear stresses for the spring, using Equation 20.17. The value of τ_{min} may be calculated from Equations 20.17 and 20.13 inasmuch as the minimum δ_c is known (i.e., $\delta_{ic} = 0.060$ in.). A shear modulus of 11.5×10^6 psi (79 GPa) will be assumed for the steel; this is the room-temperature value, which is also valid at the 80°C service temperature. Thus, τ_{min} is just

$$\tau_{\text{min}} = \frac{\delta_{ic} G d}{\pi D^2} K_w \tag{20.22a}$$

$$= \frac{\delta_{ic} G d}{\pi D^2}\left[1.60\left(\frac{D}{d}\right)^{-0.140}\right]$$

$$= \left[\frac{(0.060\ \text{in.})\,(11.5 \times 10^6\ \text{psi})\,(0.170\ \text{in.})}{\pi\,(1.062\ \text{in.})^2}\right]\left[1.60\left(\frac{1.062\ \text{in.}}{0.170\ \text{in.}}\right)^{-0.140}\right]$$

$$= 41{,}000\ \text{psi}\ (280\ \text{MPa})$$

Now τ_{max} may be determined taking $\delta_c = \delta_{mc} = 0.135$ in. as follows:

$$\tau_{\text{max}} = \frac{\delta_{mc} G d}{\pi D^2}\left[1.60\left(\frac{D}{d}\right)^{-0.140}\right] \tag{20.22b}$$

$$= \left[\frac{(0.135\ \text{in.})\,(11.5 \times 10^6\ \text{psi})\,(0.170\ \text{in.})}{\pi\,(1.062\ \text{in.})^2}\right]\left[1.60\left(\frac{1.062\ \text{in.}}{0.170\ \text{in.}}\right)^{-0.140}\right]$$

$$= 92{,}200\ \text{psi}\ (635\ \text{MPa})$$

Now, from Equation 20.21,

$$\begin{aligned} \tau_m &= \frac{\tau_{\text{min}} + \tau_{\text{max}}}{2} \\ &= \frac{41{,}000\ \text{psi} + 92{,}200\ \text{psi}}{2} = 66{,}600\ \text{psi}\ (460\ \text{MPa}) \end{aligned}$$

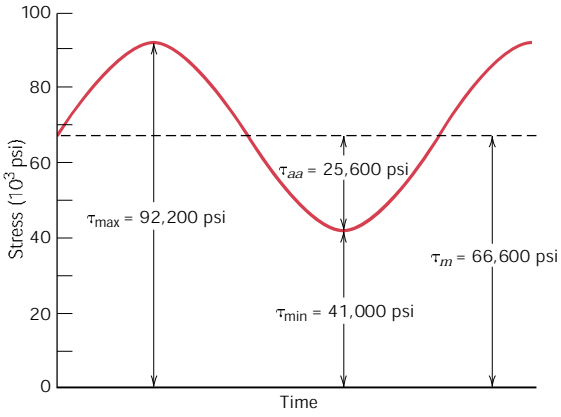

FIGURE 20.10 Shear stress versus time for an automobile valve spring.

The variation of shear stress with time for this valve spring is noted in Figure 20.10; the time axis is not scaled, inasmuch as the time scale will depend on engine speed.

Our next objective is to determine the fatigue limit amplitude (τ_{al}) for this τ_m = 66,600 psi (460 MPa) using Equation 20.19 and for τ_e and TS values of 45,000 psi (310 MPa) and 227,200 psi (1570 MPa), respectively. Thus,

$$\tau_{al} = \tau_e \left[1 - \frac{\tau_m}{0.67\,TS}\right]$$

$$= (45{,}000 \text{ psi}) \left[1 - \frac{66{,}600 \text{ psi}}{(0.67)\,(227{,}200 \text{ psi})}\right]$$

$$= 25{,}300 \text{ psi } (175 \text{ MPa})$$

Now let us determine the actual stress amplitude τ_{aa} for the valve spring using Equation 9.23 modified to the shear stress condition:

$$\tau_{aa} = \frac{\tau_{max} - \tau_{min}}{2}$$

$$= \frac{92{,}200 \text{ psi} - 41{,}000 \text{ psi}}{2} = 25{,}600 \text{ psi } (177 \text{ MPa}) \tag{20.23}$$

Thus, the actual stress amplitude is slightly greater than the fatigue limit, which means that this spring design is marginal.

The fatigue limit of this alloy may be increased to greater than 25,300 psi (175 MPa) by shot peening, a procedure described in Section 9.14. Shot peening involves the introduction of residual compressive surface stresses by plastically deforming outer surface regions; small and very hard particles are projected onto the surface at high velocities. This is an automated procedure commonly used to improve the fatigue resistance of valve springs; in fact, the spring shown in Figure 20.7 has been shot peened, which accounts for its rough surface texture. Shot peening has been observed to increase the fatigue limit of steel alloys in excess of 50% and, in addition, to reduce significantly the degree of scatter of fatigue data.

This spring design, including shot peening, may be satisfactory; however, its adequacy should be verified by experimental testing. The testing procedure is relatively complicated and, consequently, will not be discussed in detail. In essence, it

involves performing a relatively large number of fatigue tests (on the order of 1000) on this shot-peened ASTM 232 steel, in shear, using a mean stress of 66,600 psi (460 MPa) and a stress amplitude of 25,600 psi (177 MPa), and for 10^6 cycles. On the basis of the number of failures, an estimate of the survival probability can be made. For the sake of argument, let us assume that this probability turns out to be 0.99999; this means that one spring in 100,000 produced will fail.

Suppose that you are employed by one of the large automobile companies that manufactures on the order of 1 million cars per year, and that the engine powering each automobile is a six-cylinder one. Since for each cylinder there are two valves, and thus two valve springs, a total of 12 million springs would be produced every year. For the above survival probability rate, the total number of spring failures would be approximately 120, which also corresponds to 120 engine failures. As a practical matter, one would have to weigh the cost of replacing these 120 engines against the cost of a spring redesign.

Redesign options would involve taking measures to reduce the shear stresses on the spring, by altering the parameters in Equations 20.13 and 20.17. This would include either (1) increasing the coil diameter D, which would also necessitate increasing the wire diameter d, or (2) increasing the number of coils N_c.

ARTIFICIAL TOTAL HIP REPLACEMENT

20.6 Anatomy of the Hip Joint

As a prelude to discussing the artificial hip, let us first briefly address some of the anatomical features of joints in general and the hip joint in particular. The joint is an important component of the skeletal system. It is located at bone junctions, where loads may be transmitted from bone to bone by muscular action; this is normally accompanied by some relative motion of the component bones. Bone tissue is a complex natural composite consisting of soft and strong protein collagen and brittle apatite, which has a density between 1.6 and 1.7 g/cm^3. Being an anisotropic material, the mechanical properties of bone differ in longitudinal (axial) and transverse (radial) directions (Table 20.3). The articulating (or connecting) surface of each joint is coated with cartilage, which consists of body fluids that lubricate

Table 20.3 Mechanical Characteristics of Human Long Bone Both Parallel and Perpendicular to the Bone Axis

Property	*Parallel to Bone Axis*	*Perpendicular to Bone Axis*
Elastic modulus, GPa (psi)	17.4 (2.48×10^6)	11.7 (1.67×10^6)
Ultimate strength, tension, MPa (ksi)	135 (19.3)	61.8 (8.96)
Ultimate strength, compression, MPa (ksi)	196 (28.0)	135 (19.3)
Elongation at fracture	3–4%	—

Source: From D. F. Gibbons, ''Biomedical Materials,'' pp. 253–254, in *Handbook of Engineering in Medicine and Biology,* D. G. Fleming, and B. N. Feinberg, CRC Press, Boca Raton, Florida, 1976. With permission.

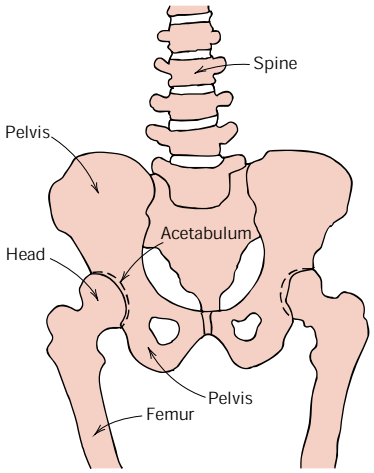

FIGURE 20.11 Schematic diagram of human hip joints and adjacent skeletal components.

and provide an interface having a very low coefficient of friction so as to facilitate the bone-sliding movement.

The human hip joint (Figure 20.11) occurs at the junction between the pelvis and the upper leg (thigh) bone, or femur. A relatively large range of rotary motion is permitted at the hip by a ball-and-socket type of joint; the top of the femur terminates in a ball-shaped head that fits into a cuplike cavity (the acetabulum) within the pelvis. An x-ray of a normal hip joint is shown in Figure 20.12*a*.

This joint is susceptible to fracture, which normally occurs at the narrow region just below the head. An x-ray of a fractured hip is shown in Figure 20.12*b*; the arrows show the two ends of the fracture line through the femoral neck. Furthermore, the hip may become diseased (osteoarthritis); in such a case small lumps of bone form on the rubbing surfaces of the joint, which causes pain as the head rotates in the

FIGURE 20.12 X-Rays of (*a*) a normal hip joint and (*b*) a fractured hip joint. The arrows in (*b*) show the two ends of the fracture line through the femoral neck.

(a) (b)

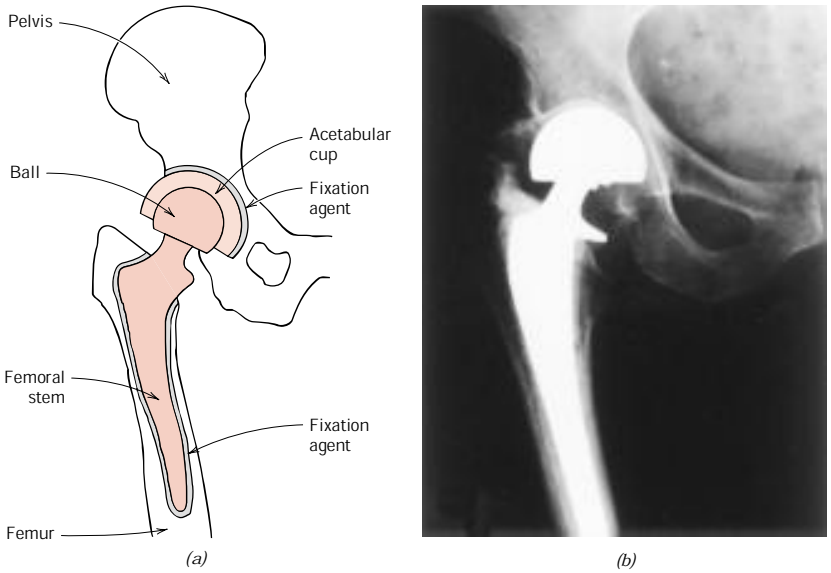

FIGURE 20.13
(*a*) Schematic diagram and (*b*) x-ray of an artificial total hip replacement.

acetabulum. Damaged and diseased hip joints have been replaced with artificial or prosthetic ones, with moderate success, beginning in the late 1950s. Total hip replacement surgery involves the removal of the head and the upper portion of the femur, and some of the bone marrow at the top of the remaining femur segment. Into this hole within the center of the femur is secured a metal anchorage stem onto which is attached, at its other end, the ball portion of the joint. In addition, the replacement cup socket must be attached to the pelvis. This is accomplished by removal of the old cup and its surrounding bone tissue. The new socket is affixed into this recess. A schematic diagram of the artificial hip joint is presented in Figure 20.13*a*; and Figure 20.13*b* shows an x-ray of a total hip replacement. In the remainder of this section we discuss material constraints and those materials that have been used with the greatest degree of success for the various artificial hip components.

20.7 Material Requirements

In essence, there are four basic components to the artificial hip: (1) the femoral stem, (2) the ball that attaches to this stem, (3) the acetabular cup that is affixed to the pelvis, and (4) a fixation agent that secures the stem into the femur and the cup to the pelvis. The property constraints on the materials to be used for these elements are very stringent because of the chemical and mechanical complexity of the hip joint. Some of the requisite material characteristics will now be discussed.

Whenever any foreign material is introduced into the body environment, rejection reactions occur. The magnitude of rejection may range from mild irritation or inflammation to death. Any implant material must be *biocompatible,* that is, it must produce a minimum degree of rejection. Products resulting from reactions with body fluids must be tolerated by the surrounding body tissues such that normal tissue function is unimpaired. Biocompatibility is a function of the location of the implant, as well as of its chemistry and shape.

The body fluid consists of an aerated and warm solution containing approximately 1 wt% NaCl in addition to other salts and organic compounds in relatively

minor concentrations. Thus, the body fluids are very corrosive, which, for metal alloys can lead not only to uniform corrosion, but also to crevice attack and pitting and, when stresses are present, to fretting, stress corrosion cracking, and corrosion fatigue. It has been estimated that the maximum tolerable corrosion rate for implant metal alloys is on the order of 0.01 mil per year (2.5×10^{-4} mm per year).

Another adverse consequence of corrosion is the generation of corrosion products that are either toxic or interfere with normal body functions. These substances are rapidly transported throughout the body; some may segregate in specific organs. Even though others may be excreted from the body, they may nevertheless still persist in relatively high concentrations by virtue of the ongoing corrosion process.

The bones and replacement components within the hip joint must support forces that originate from without the body, such as those due to gravity; in addition, they must transmit forces that result from muscular action such as walking. These forces are complex in nature and fluctuate with time in magnitude, in direction, and in rate of application. Thus, mechanical characteristics such as modulus of elasticity, yield strength, tensile strength, fatigue strength, fracture toughness, and ductility are all important considerations relative to the materials of choice for the prosthetic hip. For example, the material used for the femoral stem should have minimum yield and tensile strengths of approximately 500 MPa (72,500 psi) and 650 MPa (95,000 psi), respectively, and a minimum ductility of about 8%EL. In addition, the fatigue strength (for bending stresses that are fully reversed [Figure 9.23*a*]) should be at least 400 MPa (60,000 psi) at 10^7 cycles. For the average person, the load on the hip joint fluctuates on the order of 10^6 times per year. Furthermore, the modulus of elasticity of the prosthetic material should match that of bone; a significant difference can lead to deterioration of the bone tissue surrounding the implant.

Furthermore, since the ball-and-cup articulating surfaces rub against one another, wear of these surfaces is minimized by the employment of very hard materials. Excessive and uneven wear can lead to a change in shape of the articulating surfaces and cause the prosthesis to malfunction. In addition, particulate debris will be generated as the articulating surfaces wear against one another; accumulation of this debris in the surrounding tissues can also lead to inflammation.

Frictional forces at these rubbing counterfaces should also be minimized to prevent loosening of the femoral stem and acetabular cup assembly from their positions secured by the fixation agent. If these components do become loose over time, the hip will experience premature degradation that may require it to be replaced.

Three final important material factors are density, property reproducibility, and cost. It is highly desirable that lightweight components be used, that material properties from prosthesis to prosthesis remain consistent over time, and, of course, that the cost of the prosthesis components be reasonable.

Ideally, an artificial hip that has been surgically implanted should function satisfactorily for the lifetime of the recipient and not require replacement. For current designs, lifetimes range between only five and ten years; certainly longer ones are desirable.

Several final comments are in order relative to biocompatibility assessment. Biocompatibility of materials is usually determined empirically; that is, tests are conducted wherein materials are implanted in laboratory animals and the biocompatibility of each material is judged on the basis of rejection reactions, level of corrosion, generation of toxic substances, etc. This procedure is then repeated on humans for those materials that were found to be relatively biocompatible in ani-

mals. It is difficult to *a priori* predict the biocompatibility of a material. For example, mercury, when ingested into the body, is poisonous; however, dental amalgams, which have high mercury contents, have generally been found to be very biocompatible.

20.8 Materials Employed

FEMORAL STEM AND BALL

Early prosthetic hip designs called for both the femoral stem and ball to be of the same material—a stainless steel. Subsequent improvements have been introduced, including the utilization of materials other than stainless steel and, in addition, constructing the stem and ball from different materials. Figure 20.14 is a photograph in which are shown two different hip replacement designs.

Currently, the femoral stem is constructed from a metal alloy of which there are three possible types: stainless steel, cobalt–nickel–chromium–molybdenum, and titanium. The most suitable stainless steel is 316L, which has a very low sulfur content ($<$0.002 wt%); its composition is given in Table 13.4. The principal disadvantages of this alloy are its susceptibility to crevice corrosion and pitting, and its relatively low fatigue strength. Fabrication technique may also have a significant influence on its characteristics. Cast 316L typically has poor mechanical properties and inadequate corrosion resistance. Consequently, prosthetic femoral stems are either forged or cold worked. Furthermore, heat treatment may also influence the characteristics of the material and must be taken into consideration. Normally, 316L is implanted in older and less active persons. The mechanical characteristics and corrosion rate range of this alloy (in the cold-worked state) are supplied in Table 20.4.

Various Co–Cr–Mo and Co–Ni–Cr–Mo alloys have been employed for artificial hip prostheses; one that has been found to be especially suitable, designated MP35N, has a composition of 35 wt% Co, 35 wt% Ni, 20 wt% Cr, and 10 wt% Mo. It is formed by hot forging and, as such, has tensile and yield strengths that are superior to 316L stainless steel (Table 20.4). Furthermore, its corrosion and fatigue characteristics are excellent.

Of those metal alloys that are implanted for prosthetic hip joints, probably the most biocompatible is the titanium alloy Ti–6Al–4V; its composition is 90 wt% Ti, 6 wt% Al, and 4 wt% V. The optimal properties for this material are produced by hot forging; any subsequent deformation and/or heat treatment should be avoided

Figure 20.14 Photograph showing two artificial total hip replacement designs.

Table 20.4 Mechanical and Corrosion Characteristics of Three Metal Alloys That Are Commonly Used for the Femoral Stem Component of the Prosthetic Hip

Alloy	*Elastic Modulus [GPa (psi)]*	*0.2% Yield Strength [MPa (ksi)]*	*Tensile Strength [MPa (ksi)]*	*Elongation at Fracture (%)*	*Fatigue Strength or Limit, 10^7 Cycles [MPa (ksi)]*	*Corrosion Rate (mpy)*[a]
316L Stainless steel (cold worked)	196 (28.4×10^6)	700 (102)	875 (127)	12	383 (55.5)	0.001–0.002
MP35N (hot forged)	230 (33.4×10^6)	1000 (145)	1200 (174)	13	500 (72.5)	0.0012–0.002
Ti-6Al-4V (hot forged)	120 (17.4×10^6)	950 (138)	1075 (156)	13	580 (84.1)	0.007–0.04

[a] mpy means mils per year, or 0.001 in./yr

Sources: From Gladius Lewis, *Selection of Engineering Materials,* © 1990, p. 189. Adapted by permission of Prentice Hall, Englewood Cliffs, New Jersey. And D. F. Gibbons, ''Materials for Orthopedic Joint Prostheses,'' Ch. 4, p. 116, in *Biocompatibility of Orthopedic Implants,* Vol. I, D. F. Williams, CRC Press, Boca Raton, Florida, 1982. With permission.

to prevent the formation of microstructures that are deleterious to its bioperformance. The properties of this alloy are also listed in Table 20.4.

Recent improvements for this prosthetic device include using a ceramic material for the ball component rather than any of the aforementioned metal alloys. The ceramic of choice is a high-purity and polycrystalline aluminum oxide, which is harder and more wear resistant, and generates lower frictional stresses at the joint. However, the fracture toughness of alumina is relatively low and its fatigue characteristics are poor. Hence, the femoral stem, being subjected to significant stress levels, is still fabricated from one of the above alloys, and is then attached to the ceramic ball; this femoral stem–ball component thus becomes a two-piece unit.

The materials selected for use in an orthopedic implant come after years of research into the chemical and physical properties of a host of different candidate materials. Ideally, the material(s) of choice will not only be biocompatible, but have mechanical properties that match the biomaterial being replaced—viz., bone. However, no man-made material is both biocompatible and possesses the property combination of bone and the natural hip joint—i.e., low modulus of elasticity, relatively high strength and fracture toughness, low coefficient of friction, and excellent wear resistance. Consequently, material property compromises and trade-offs must be made. For example, recall that the modulus of elasticity of bone and femoral stem materials should be closely matched such that accelerated deterioration of the bone tissue adjacent to the implant is avoided. Unfortunately, man-made materials that are both biocompatible and relatively strong, also have high moduli of elasticity. Thus, for this application, it was decided to trade off a low modulus for biocompatibility and strength.

ACETABULAR CUP

Some acetabular cups are made from one of the biocompatible alloys or aluminum oxide. More commonly, however, ultrahigh molecular weight polyethylene (Section 13.16) is used. This material is virtually inert in the body environment and has excellent wear-resistance characteristics; furthermore, it has a very low coefficient of friction when in contact with the materials used for the ball component of the socket.

FIXATION

Successful performance of the artificial hip joint calls for the secure attachment of both the femoral stem to the femur and the acetabular cup to the pelvis. Insecure attachment of either component ultimately leads to a loosening of that component and the accelerated degradation of the joint. A fixation agent is sometimes used to bond these two prosthetic components to their surrounding bone structures. The most commonly used fixation agent is a polymethyl methacrylate (acrylic) bone cement that is polymerized *in situ* during surgery.

This acrylic bond cement has, in some cases, contributed to femoral stem loosening because it is brittle and does not bond well with the metallic implant and bone tissue. It has been found that a more secure implant–bone bond is formed when the stem is coated with a porous surface layer, consisting of a sintered metal powder. After implantation, bone tissue grows into the three-dimensional pore network, and thereby fixates the implant to the bone. Such a coating has been applied to the upper stem region of the right hip replacement shown in Figure 20.14.

THERMAL PROTECTION SYSTEM ON THE SPACE SHUTTLE ORBITER

20.9 Introduction

In 1969, the National Aeronautics and Space Administration (NASA) of the United States decided to direct its primary mission to the development of a *Space Transportation System* (*STS*), also commonly known as the *Space Shuttle Orbiter*. In essence, the Space Shuttle is a reusable cargo-carrying space vehicle that is launched aboard a rocket, and then orbits the earth. Upon mission completion, it reenters the atmosphere as a space craft, and, finally, once inside the lower atmosphere, lands in the manner of a normal aircraft. The maiden flight was made by the *Columbia* orbiter in April of 1981; since then, four other orbiters have been constructed—*Discovery*, *Atlantis*, *Endeavour*, and the ill-fated *Challenger*. A photograph of the *Atlantis* is shown in the chapter-opening photograph for this chapter.

The successful operation of the Space Shuttle is dependent on a fully reusable outer ''skin,'' termed a *Thermal Protection System* (*TPS*), that protects the inner airframe and its occupants from the searing heat generated during the reentry phase from space into the earth's atmosphere. The development of this Thermal Protection System evolved over a twenty-year period, and is a classical and somewhat involved materials selection and design problem. In this section the primary components of the Shuttle's TPS are discussed.

In reading this section, keep in mind that cost constraints relative to the design and fabrication of these materials were not as rigid as would be expected for normal commercial applications.

20.10 Thermal Protection System—Design Requirements

Material requirements on the Thermal Protection System are, to say the least, awesome. For example, the TPS must do the following:

1. Maintain the temperature on the inner airframe below that to which it was designed [viz., 175°C (350°F)] for a maximum outer surface temperature of 1260°C (2300°F).

2. Remain usable for 100 missions, with a maximum turnaround time of 160 h.
3. Provide and maintain an aerodynamically smooth outer surface.
4. Be constructed of low-density materials.
5. Withstand temperature extremes between −110°C (−170°F) and 1260°C (2300°F).
6. Be resistant to severe thermal gradients and rapid temperature changes.
7. Be able to withstand stresses and vibrations that are experienced during launch, as well as thermally induced stresses imposed during temperature changes.
8. Experience a minimum absorption of moisture and other contaminants during storage between missions.
9. Be made to adhere to the airframe that is constructed of an aluminum alloy.

Thermal protection systems and materials developed previously by the aerospace industry proved unsuitable for the Space Shuttle because they were either too dense and/or nonreusable. Therefore, it became necessary to design a new set of complex materials. Furthermore, no single material is capable of meeting all of the criteria listed above. In addition, not all of these criteria are required over all surfaces of the spacecraft; for example, typical reentry maximum temperature profiles are shown in Figure 20.15.

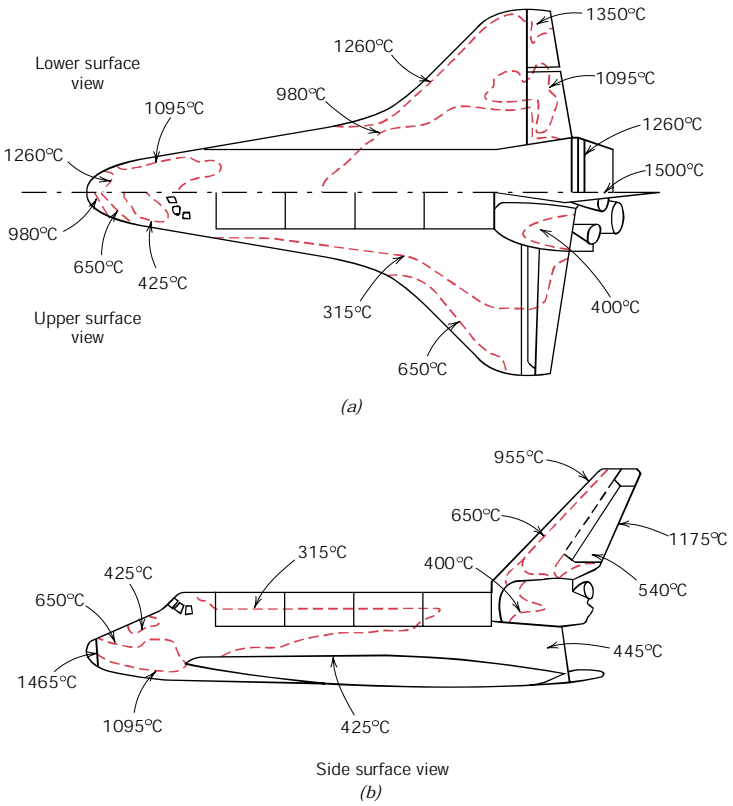

FIGURE 20.15 Approximate maximum outer surface temperature profiles for the Space Shuttle Orbiter during reentry: (*a*) upper and lower views; (*b*) side view. (From "The Shuttle Orbiter Thermal Protection System," L. J. Korb, C. A. Morant, R. M. Calland, and C. S. Thatcher, *Ceramic Bulletin*, No. 11, Nov. 1981, p. 1188. Copyright 1981. Reprinted by permission of the American Ceramic Society.)

Table 20.5 Thermal Protection Systems Employed on the Space Shuttle Orbiter

Material Generic Name	*Minimum Operating Temperature, °C (°F)*	*Maximum Operating Temperature, °C (°F)*	*Material Composition*	*Orbiter Locations*
Felt reusable surface insulation (FRSI)	−130 (−200)	400 (750)	Nylon felt, silicone rubber coating	Wing upper surface, upper sides, cargo bay doors
Advanced flexible reusable surface insulation (AFRSI)	−130 (−200)	815 (1500)	Quartz batting sandwiched between quartz and glass fabrics	Upper surface regions
Low-temperature reusable surface insulation (LRSI)	−130 (−200)	650 (1200)	Silica tiles, borosilicate glass coating	Upper wing surfaces, tail surfaces, upper vehicle sides
High-temperature reusable insulation (HRSI)	−130 (−200)	1260 (2300)	Silica tiles, borosilicate glass coating with SiB_4 added	Lower surfaces and sides, tail leading and trailing edges
Reinforced carbon–carbon (RCC)	No lower limit identified	1650 (3000)	Pyrolized carbon–carbon, coated with SiC	Nose cap and wing leading edges

Source: Adapted from L. J. Korb, C. A. Morant, R. M. Calland and C. S. Thatcher, ''The Shuttle Orbiter Thermal Protection System,'' *Ceramic Bulletin*, No. 11, Nov. 1981, p. 1188. Copyright 1981. Reprinted by permission of the American Ceramic Society.

Therefore, the philosophy adopted was to design several different thermal protection materials systems, each with its particular set of properties, that satisfy the required criteria for a specific region of the spacecraft surface. Several different materials systems are employed on the Space Shuttles, the designs of which depend on the maximum outer surface temperature generated during vehicle reentry. These systems and their temperature ranges of operation, material compositions, and orbiter areas are listed in Table 20.5. Furthermore, the locations of these various systems are indicated in Figure 20.16.

20.11 Thermal Protection System—Components

FELT REUSABLE SURFACE INSULATION

Upper surface regions exposed up to temperatures of 400°C (750°F) are covered with what is termed *felt reusable surface insulation* (*FRSI*). This insulation consists of felt blankets of a nylon material the outer surface of which is coated with a silicone elastomer to achieve the necessary surface thermal properties. These blankets come in two thicknesses, 4 and 8 mm (0.16 and 0.32 in.), and are bonded to the aluminum airframe by a room-temperature vulcanizing (RTV) silicone adhesive.

Other upper surface regions that are exposed to higher temperatures, not to exceed 815°C (1500°F), are protected by blankets of an *advanced flexible reusable surface insulation (AFRSI)*. These blankets consist of a quartz fiber batting that is sandwiched between a high-temperature woven quartz fabric on the outer side and a lower-temperature glass fabric on the inner side. The outer surface of some regions is also protected with a ceramic coating. Furthermore, these three layers are stitched together using quartz and glass threads in a one-inch square pattern.

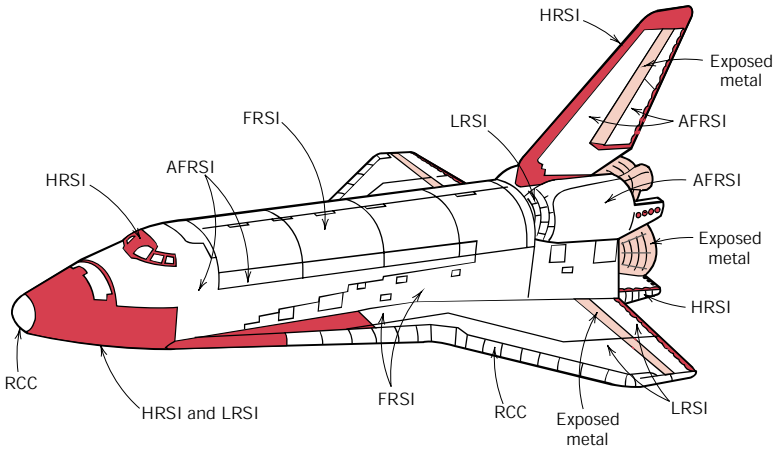

FIGURE 20.16 Locations of the various components of the thermal protection system on the Space Shuttle Orbiter: FRSI, felt reusable surface insulation; AFRSI, advanced flexible reusable surface insulation; LRSI, low-temperature reusable surface insulation; HRSI, high-temperature reusable surface insulation; RCC, reinforced carbon–carbon composite. (Adapted from L. J. Korb, C. A. Morant, R. M. Calland, and C. S. Thatcher, "The Shuttle Orbiter Thermal Protection System," *Ceramic Bulletin*, No. 11, Nov. 1981, p. 1189. Copyright 1981. Reprinted by permission of the American Ceramic Society.)

AFRSI blanket thicknesses range between 10 mm (0.41 in.) and just under 50 mm (2 in.). Over most vehicle regions, these AFRSI blankets are bonded to the structure by a silicone RTV adhesive, as with the FRSI insulation.

CERAMIC TILE SYSTEMS

More rigid material restrictions are imposed on regions of the Space Shuttle that are exposed to temperatures in the range of 400 to 1260°C (750 to 2300°F). For these areas it was decided to use a relatively complex ceramic material in the form of tiles. Ceramics are intrinsically thermal insulators and, furthermore, will withstand these elevated temperatures. The tile design is utilized for the protection system to conform to the contours of the Shuttle's surface, and also to accommodate the thermal dimensional changes accompanying the extremes of temperature that are experienced during a typical mission.

Each Shuttle has on the average of 24,300 of these tiles, which comprise approximately 70% of the total orbiter exterior area. No two tiles have exactly the same configuration, but sizes range from between about 150 mm by 150 mm (6 in. by 6 in.) to about 200 mm by 200 mm (8 in. by 8 in.). Tile thicknesses vary between 5 mm (0.2 in.) and 90 mm (3.5 in.). Each tile is precisely machined to its individual shape using diamond tools on a computer-controlled mill. Figure 20.17 is a photograph that shows the tiles being installed.

Tiles having three densities are used, which are designated by LI-900, FRCI-12, and LI-2200; the respective densities of these materials are 0.14 g/cm^3 (9 lb$_m$/ft^3), 0.19 g/cm^3 (12 lb$_m$/ft^3), and 0.35 g/cm^3 (22 lb$_m$/ft^3). The LI-900 and LI-2200 materials are fabricated using very high-purity silica fibers, having diameters ranging between 1 and 4 μm and lengths on the order of 3 mm (0.13 in.). Fiber-to-fiber bonds are established by a sintering heat treatment at 1370°C (2500°F), which gives